



PACIFIC EARTHQUAKE ENGINEERING RESEARCH CENTER

Ground Motions for Site Response Estimates —1906 Earthquake

Paul Somerville

Robert Graves

Nancy Collins

URS Greiner Woodward Clyde
Pasadena, California

**A report to the PEER Program of
Applied Earthquake Engineering Research on
Lifeline Systems**

**The financial support of the sponsor organizations including
the Pacific Gas & Electric Company (PG&E),
the California Energy Commission (CEC), and the
California Department of Transportation (Caltrans) is acknowledged.**

PG&E-PEER DIRECTED STUDIES PROGRAM, PHASE II

**SIMULATED TIME HISTORY OF THE 1906 SAN FRANCISCO
EARTHQUAKE AT COYOTE CREEK, SAN JOSE**

TASK 5C FINAL REPORT

JUNE 6, 2000

Paul Somerville, Robert Graves, Nancy Collins

URS Corporation, Pasadena, CA.

INTRODUCTION

This report describes the generation of a ground motion time history of the 1906 earthquake that represents the ground motions experienced at Coyote Creek, San Jose. The time history was generated using a broadband simulation procedure that is summarized in the following section and described in detail in the Appendix. The simulated ground motions are representative of stiff alluvial site conditions. The source rupture model of the 1906 San Francisco earthquake used in the simulation was derived from the model of Wald et al. (1993). The Coyote Creek site is located at Lat. 37 degrees 25.609 minutes north, 121 degrees 55.643 minutes west, North American datum 1927. The site is about 20.9 km northeast of the San Andreas fault, between the epicenter and the southern termination of rupture at San Juan Bautista, as shown in Figure 1.

The ground motions at the Coyote Creek site have moderate amplitudes because the site is located near a part of the fault that had low slip, and because it is located relatively close to the epicenter of the earthquake, and thus has moderate rupture directivity effects. For these reasons, the ground motions that were simulated at the Coyote Creek site are not representative of the ground motions of the 1906 earthquake at a distance of 20.9 km from the fault, especially in the region north of the San Francisco Bay.

SOURCE MODEL OF THE 1906 SAN FRANCISCO EARTHQUAKE

A rupture model of the 1906 San Francisco earthquake derived from teleseismic data by Wald et al. (1993) is shown in Figure 2. This figure also shows a comparison of the fault slip inferred from the teleseismic data with the geologically and geodetically measured fault slip. The overall rupture length of the earthquake was 340 km. The hypocenter of the earthquake was assumed to be in Daly City, based on Bolt (1968) and Boore (1977). The largest concentration of slip occurred well north of the epicenter, between Point Reyes and Fort Ross. A smaller concentration of slip occurred immediately south of the epicenter in Daly City.

Experience in the analysis of ground motions from well recorded strike-slip earthquakes, such as the 1989 Loma Prieta and 1995 Kobe earthquakes (Wald et al.,

1991, Figure 11; Wald, 1996, Figure 11), shows that the strong motions experienced at a site are dominated by the part of the rupture that lies between the epicenter and the site. This is especially true of rupture directivity effects, which influence the ground motions at periods longer than about 0.5 seconds. Our simulations confirm our expectation that the only part of the 1906 fault rupture that produced significant ground motion levels at the Coyote Creek site is the segment that lies between the epicenter and San Juan Bautista. According to the Wald et al. (1993) rupture model, the slip on the San Andreas fault was about 6.5 meters at the epicenter of the 1906 earthquake, and decreased steadily to zero about 70 km southeast of the epicenter. At the closest point on the fault to the Coyote Creek site, the slip was less than 2 meters. The region of large slip between Point Reyes and Fort Ross, characterized by fault slip of as much as 10 meters, is located more than 150 km from the site.

The fault parameters used in the simulation are summarized in Table 2. We modeled a 260 km long segment of the rupture that contains almost all of the seismic moment of the earthquake. The 80 km segment at the northwestern part of the fault, which was not included in the rupture model used in the ground motion simulations, would have a negligible effect on the ground motions at Coyote Creek. We used the scaling relations for crustal earthquakes developed by Somerville et al. (1999) to estimate a rise time of 3.2 seconds. The sensitivity of simulated ground motions to the source parameters of large San Andreas earthquakes has been investigated by Graves (1998).

Table 1. Source Parameters for the 1906 San Francisco Earthquake Simulation

PARAMETER	VALUE
Seismic Moment	3.3×10^{27} dyne cm
Mw	7.65
Length	260 km
Width	12 km
Depth to Top	1.5 km
Strike	141
Dip	90
Rake	180
Hypocenter	37.67N, 122.46 E, 8 km depth
Length northwest of epicenter	165 km
Length southwest of epicenter	95 km
Rupture velocity	2.7 km/sec
Rise Time	3.22 sec
Slip Model, Crustal Velocity Model	Wald et al., 1991

BROADBAND SIMULATION METHOD

The broadband ground motion simulation procedure is a hybrid procedure that computes the low frequency and high frequency ranges separately and then combines the two to produce a single time history. At frequencies below 1 Hz, it contains a theoretically rigorous representation of radiation pattern, rupture directivity and wave propagation effects, and reproduces recorded ground motion waveforms and amplitudes.

At frequencies above 1 Hz, it uses a theoretically rigorous representation of wave propagation effects which is combined with theoretically-based semi-empirical representations of stochastic processes including source radiation pattern and scattering in the path and site. The simulation procedure has been calibrated against the recorded strong motions from numerous earthquakes.

The synthetic seismogram procedure that we use to generate the low frequency part of the broadband seismogram is described by Hartzell and Heaton (1983). It is implemented using frequency-wavenumber integration to compute Green's functions which are convolved with the slip function on the fault. The high frequency ground motion simulation procedure that we use is described by Wald et al. (1988) and Somerville (1993). It is implemented using a generalized ray method to calculate simplified Green's functions, which are convolved with empirical source functions derived from near-fault strong motion recordings of small earthquakes. The low frequency and high frequency parts of the simulation are combined using matched filters, as described by Somerville et al. (1995a,b). An outline of the procedure is given in the following paragraphs.

The fault model is specified as a finite rectangular fault surface that is divided into discrete sub-fault elements, and the motions from these elements are summed and lagged to simulate the propagation of rupture over the fault surface. The parameters required for specifying the source are seismic moment, fault length, fault width, strike, dip, rake, depth of top of fault, hypocenter, rupture velocity, and slip distribution (which may include spatially variable rake and time function of slip). Radiation pattern and fault subevents are treated differently in two different frequency ranges. At low frequencies (<1 Hz), the fault is discretized finely enough to produce a continuous slip function for frequencies below one second, and the theoretical radiation pattern is used. At high frequencies (>1 Hz), the fault is discretized into sub-fault elements having dimensions of several km. The radiation of seismic waves from these sub-fault elements is represented by empirical source functions, which are recorded accelerograms of events having the dimensions of the fault elements (magnitude ~ 5 earthquakes) that have been corrected back to the source. The radiation pattern is represented empirically by selecting source functions having the required theoretical radiation pattern value for each sub-fault element. We have used empirical source functions derived from an aftershock of the 1979 Imperial Valley earthquake.

The modeling of wave propagation effects requires the specification of seismic velocities, density, and Q of a flat layered crustal model. We have used the velocity model used by Wald et al. (1991) in modeling the 1989 Loma Prieta earthquake. Path effects are treated differently in these two different frequency ranges. At low frequencies (<1 Hz), path effects are represented by Green's functions calculated using an efficient frequency-wavenumber integration scheme (Saikia, 1994). These Green's functions contain the complete response of the anelastic layered medium (all body wave and surface wave phases) for frequencies below a given value (typically chosen to be 5 Hz). They also contain the near-field term in addition to the far-field term, and include the static displacement field of the earthquake. At high frequencies (>1 Hz), path effects are represented by simplified Green's functions calculated using generalized ray theory (Helmberger and Harkrider, 1978). These Green's functions are accurate up to indefinitely high frequencies (typically 50 Hz), and contain all of the significant rays.

They are simplified in the sense that they do not include the radiation pattern and the receiver function. The simplified Green's functions are used to transfer the empirical source functions from the depth, horizontal range and velocity structure in which they were recorded to the depth, horizontal range and velocity structure in which they are to be used for ground motion simulation. Scattering effects in the path are represented empirically by wave propagation effects contained in the recorded source functions.

At low frequencies, site effects are incorporated by calculating Green's functions using surface velocity, density and Q appropriate for the site. For the high frequency part of the simulation, the receiver function is included empirically in the recorded source functions; the partitioning of energy among components is treated in a site-specific manner by applying a receiver function correction to the empirical source functions which rotates the recorded wave field into the appropriate partitioning for the velocity structure at the site. Scattering effects near the site are represented by wave propagation effects contained in the empirical source functions that are not modeled by the simplified Green's functions. The site attenuation contained in the empirical source functions is adjusted to provide the value that is appropriate at the site.

The ground motion model has no free parameters when used to model the recorded ground motions of an earthquake. The method has been validated against the recorded strong ground motions of numerous earthquakes, including the 1989 Loma Prieta earthquake (Somerville et al., 1994a,b). Based on this validation experience, we have documented that the ground motion simulation procedure is applicable for magnitudes in the range of 5 to 8; distances from 0 to 200 km, and frequencies between 0.2 and 35 Hz.

GROUND MOTION TIME HISTORY AT COYOTE CREEK

The north, east and vertical components of acceleration, velocity and displacement for simulated ground motion time history are shown in Figure 3. The separate contributions of the two main concentrations of slip on the fault are evident in these time histories. The asperity immediately south of the epicenter produces about 10 seconds of horizontal component acceleration with peaks of about 0.1g, a long period velocity pulse with a peak velocity of 16.5 and 12 cm/sec on the north and east components respectively, and a corresponding displacement pulse with peak displacements of about 20 and 40 cm on these two components. The asperity between Point Reyes and Fort Ross produces much smaller ground motions that arrive about one minute later. At long periods, the ground motions are much smaller because of backward

Boore (1977) described an analysis of strong motion recordings of the 1906 earthquake. The recordings were made on primitive seismographs that were all driven off scale. The clearest recording was made on a three-component Ewing instrument at Mount Hamilton (Boore, 1997, Figure 3). This recording, normalized by the static magnification of the instrument, shows clipping at about 3 cm of displacement soon after the inferred onset of the S wave. Modeling of this record is beyond the scope of the present study, but the simulations described in this report are considered to be not inconsistent with the Mount Hamilton record. The ground displacement calculations at Mount Hamilton shown by Boore (1977) in Figure 7 are quite compatible with those in

Figure 3 of this report, both in polarity and amplitude, although the calculations in this report are somewhat larger because their body waves were calculated for a layered crustal model.

The response spectra of the simulated ground motions are shown in Figure 4. These response spectra show the separate contributions of the low frequency and high frequency simulations, in addition to the response spectra of the combined broadband time histories. The simulated response spectra are compared with the prediction of the empirical model of Abrahamson and Silva (1997) for soil sites. The simulated spectra are lower than the empirical spectra at all periods. This difference may be attributable to the following factors.

The largest concentration of slip in the 1906 earthquake occurred well north of the epicenter, between Point Reyes and Fort Ross. This main asperity of the 1906 earthquake produced insignificant ground motion levels at the Coyote Creek site, because of its distance from the site (about 160 km) and because rupture of this segment propagated away from the Coyote Creek site. A smaller concentration of slip occurred immediately south of the epicenter in Daly City. The ground motions at the Coyote Creek site have moderate amplitudes because the site is located near a part of the fault that had low slip, and because it is located relatively close to the epicenter of the earthquake, and thus has moderate rupture directivity effects. For these reasons, the ground motions that were simulated at the Coyote Creek site are not representative of the ground motions of the 1906 earthquake at a distance of 20.9 km from the fault, especially in the region north of the San Francisco Bay.

There is no strong motion recording of the 1989 Loma Prieta earthquake at Coyote Creek. The closest recording site is the Milpitas site (CSMIP #57502), about 3 km east of Coyote Creek, where the instrument is located on the floor beside the wall of a two story building. The north, east and vertical components of acceleration, velocity and displacement recorded at the Milpitas site during the 1989 Loma Prieta earthquake are shown in Figure 5. The duration of the Milpitas acceleration time history is similar to that of the 1906 Coyote Creek simulation.

The response spectrum of the Milpitas recording of the 1989 Loma Prieta earthquake is compared with the response spectrum of the 1906 earthquake simulation at Coyote Creek in Figure 6. The response spectra are similar at short periods, but the Loma Prieta earthquake is larger at periods longer than about 2 seconds. This may reflect the fact that the 1989 Loma Prieta earthquake is closer to Coyote Creek than the Daly City asperity of the 1906 earthquake, although it has a smaller seismic moment (M_w 6.95 for Loma Prieta compared to M_w 7.15 for the Daly City asperity of the 1906 earthquake).

Our simulations of the 1906 earthquake at Coyote Creek are for stiff alluvial site conditions, and have not taken site specific ground conditions at Coyote Creek into account. These conditions may include the effects of the response of the Santa Clara basin, which may be significant in the Milpitas recording of the 1989 Loma Prieta earthquake. The development of reliable 3D velocity models of the Santa Clara basin may provide the means to test the modeling of Santa Clara basin effects using the Loma Prieta recordings, and the application of basin modeling to incorporate basin effects in the simulation of ground motions from the 1906 earthquake.

REFERENCES

- Abrahamson, N.A. and W.J. Silva (1997). Empirical response spectral attenuation relations for shallow crustal earthquakes. *Seismological Research Letters* 68, 94-127.
- Abrahamson, N.A., P.G. Somerville, and C. Allin Cornell (1990). Uncertainty in numerical strong motion predictions, *Proc. 4th U.S. National Conference on Earthquake Engineering*, 1, 407-416.
- Bolt, B.A. (1968). The focus of the 1906 California earthquake. *Bull. Seism. Soc. Am.* 58, 457-471.
- Boore, D.M. (1977). Strong motion recordings of the California earthquake of April 18, 1906. *Bull. Seism. Soc. Am.* 67, 561-577.
- Graves, R. (1998). Three-dimensional finite-difference modeling of the San Andreas fault: source parameterization and ground-motion levels. *Bull. Seism. Soc. Am.* 88, 881-897.
- Hartzell, S.H. and T.H. Heaton (1983). Inversion of strong ground motion and teleseismic waveform data for the fault rupture of the 1979 Imperial Valley, California earthquake, *Bull. Seism. Soc. Am.* 83, 780-810.
- Helmberger, D.V. (1983). Theory and application of synthetic seismograms. in *Earthquakes: Observation, Theory and Interpretation*, Proc. Int. Sch. Phys. "Enrico Fermi" Course LXXXV, pp. 174-221, eds. Kanamori, H. and E. Boschi, North-Holland, Amsterdam.
- Saikia, C.K. (1994a). Modified frequency-wavenumber algorithm for regional seismograms using Filon's quadrature: modeling of Lg waves in eastern North America. *Geophys. J. Int.* 118, 142-158.
- Somerville, P.G., K. Irikura, R. Graves, S. Sawada, D. Wald, N. Abrahamson, Y. Iwasaki, T. Kagawa, N. Smith and A. Kowada (1999). Characterizing crustal earthquake slip models for the prediction of strong ground motion. *Seism. Res. Lett.* 70, 59-80.
- Somerville, P.G., R.W. Graves, and C.K. Saikia (1995). Characterization of Ground Motions during the Northridge Earthquake of January 17, 1994, SAC Steel Project Report SAC 95-03.
- Somerville, P.G., N.F. Smith and R.W. Graves (1994a). The effect of critical Moho reflections on the attenuation of strong motion from the 1989 Loma Prieta, in *"The Loma Prieta, California, Earthquake of October 17, 1989 - Strong Ground Motion,"* U.S.G.S. Professional Paper 1551-A, A67-A75.
- Somerville, P.G., D.J. Wald, and N.F. Smith (1994b). Prediction of the near-source ground accelerations of the Loma Prieta earthquake using a heterogeneous slip model, unpublished manuscript.

Somerville, P., C. Saikia, D. Wald, and R. Graves (1995b). Implications of the Northridge earthquake for strong ground motions from thrust faults, *Bull. Seism. Soc. Am.* 86, Part 1, S115-S125.

Wald, D.J. (1996). Slip history of the 1995 Kobe, Japan earthquake determined from strong motion, teleseismic, and geodetic data. *J. Phys. Earth* 44, 489-503.

Somerville, P.G. (1993). Engineering applications of strong motion simulation, *Tectonophysics*, 218, 195-219.

Wald, D.J., H. Kanamori, D. Helmberger, and T.H. Heaton (1993). Source study of the 1906 San Francisco earthquake. *Bull. Seism. Soc. Am.* 83, 981-1019.

Wald, D.J., D. Helmberger, and T.H. Heaton (1991). Rupture model of the 1989 Loma Prieta earthquake from the inversion of strong-motion and broadband teleseismic data. *Bull. Seism. Soc. Am.* 81, 1540-1572.

Wald, D.J., L.J. Burdick and P.G. Somerville (1988). Simulation of acceleration time histories close to large earthquakes. *Earthquake Engineering and Soil Dynamics II - Recent Advances in Ground Motion Evaluation*, Geotechnical Special Publication 20, J. Lawrence Von Thun, ed., 430-444.

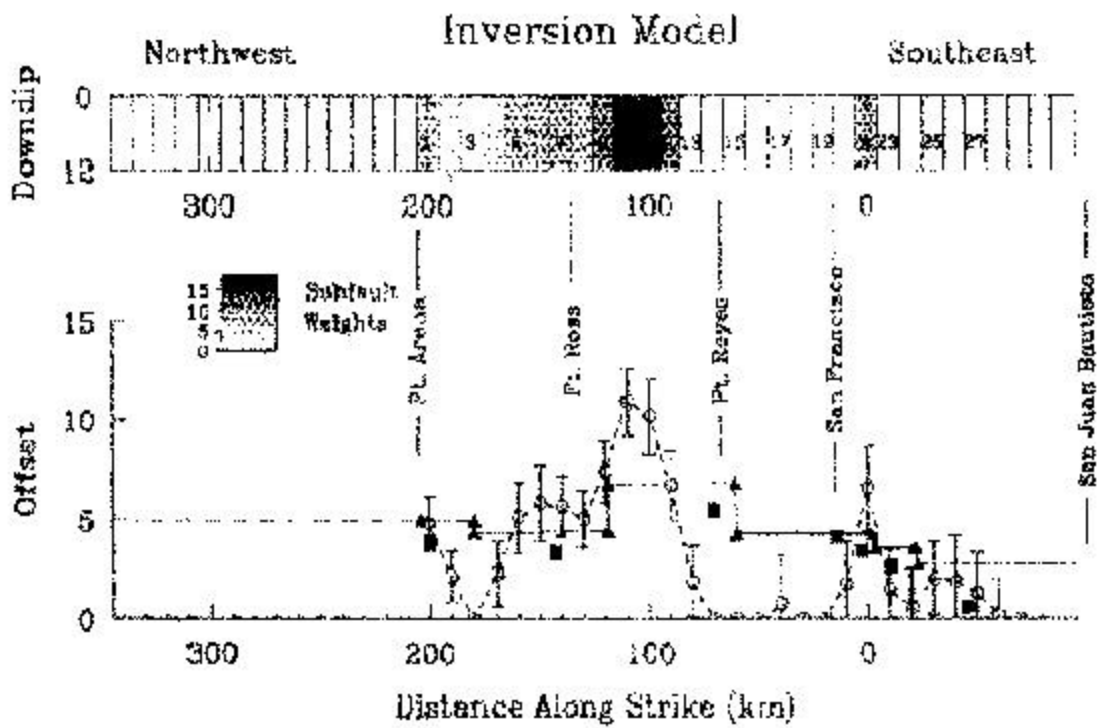


Figure 2. Rupture model of the 1966 San Francisco earthquake (top) and comparison of the slip distribution (nodes with uncertainty bars connected by a dashed line) with geodetic data (solid triangles connected by lines) and geological data (solid squares) from Thatcher, 1975. Source: Wald et al., 1993.

APPENDIX 1.

BROADBAND GROUND MOTION SIMULATION METHOD

Introduction

The broadband strong motion simulation method is a hybrid method that computes the ground motions separately in the short period and long period ranges and then combines them. We used a transition period of 1 seconds between the short period and long period ranges in the simulations described in this report; Figure A1-1 schematically shows the matched filters for a period of 3 seconds. The method used for short periods is based on the summation of strong motion recordings from smaller earthquakes. The method used for long periods is a standard method for calculating synthetic seismograms based on theoretical Green's functions. This standard method has been used extensively to successfully model the waveforms of long period strong ground motions recorded from many recent earthquakes, and is the basis for the rupture models of earthquakes that are inverted from strong motion recordings.

The fault model is specified as a finite rectangular fault surface that is divided into discrete sub-fault elements, and the motions from these elements are summed and lagged to simulate the propagation of rupture over the fault surface. The parameters required for specifying the source are seismic moment, fault length, fault width, strike, dip, rake, depth of top of fault, hypocenter, rupture velocity, and slip distribution (which may include spatially variable rake and time function of slip). Radiation pattern and fault subevents are treated differently in two different period ranges. For the long period simulation, the fault is discretized finely enough to produce a continuous slip function for periods longer than the transition period, and the theoretical radiation pattern is used.

For the short period simulation, the fault is discretized into sub-fault elements whose dimensions are chosen so as to maintain self-similarity in the spectral shape between the subevent on the fault element and the large event based on an omega-squared scaling relation (Joyner and Boore, 1986), as described by Somerville et al. (1991). The radiation of seismic waves from these sub-fault elements is represented by empirical source functions, which are recorded accelerograms of events having the dimensions of the fault elements and that have been corrected back to the source.

The modeling of wave propagation effects requires the specification of seismic velocities, density, and Q of a flat layered crustal model. Path effects are treated differently in these two different period ranges. At long periods, path effects are represented by Green's functions calculated using an efficient frequency-wavenumber integration scheme (Saikia, 1994). These Green's functions contain the complete response of the anelastic layered medium (all body wave and surface wave phases) for frequencies below a given value (typically chosen to be 5 Hz). They also contain the near-field term in addition to the far-field term, and include the static displacement field of the earthquake. At short periods, path effects are represented by simplified Green's functions calculated using generalized ray theory (Helmberger, 1983). These Green's functions are accurate up to indefinitely high frequencies (typically 50 Hz), and contain

all of the significant rays. They are simplified in the sense that they do not include the radiation pattern and the receiver function. The simplified Green's functions are used to transfer the empirical source functions from the depth, horizontal range and velocity structure in which they were recorded to the depth, horizontal range and velocity structure in which they are to be used for ground motion simulation. Scattering effects in the path are represented empirically by wave propagation effects contained in the recorded source functions.

At long periods, site effects are incorporated by calculating Green's functions using surface velocity, density and Q appropriate for the site. For the short period part of the simulation, the receiver function is included empirically in the recorded source functions; the partitioning of energy among components is treated in a site-specific manner by applying a receiver function correction to the empirical source functions which rotates the recorded wave field into the appropriate partitioning for the velocity structure at the site. Scattering effects near the site are represented by wave propagation effects contained in the empirical source functions that are not modeled by the simplified Green's functions. The site attenuation contained in the empirical source functions is adjusted to provide the value that is appropriate at the site.

In the following sections, we provide more detail about specific aspects of the broadband strong motion simulation procedure. This description addresses the earthquake source, the propagation path, and the site, and summarizes the parameters requiring specification. It also describes important features of the procedure and the validation of the procedure against recorded strong ground motions.

Source

A finite source is used. For the simulation of ground motions from an earthquake for which a rupture model has been inverted, the parameters derived from the inversion provide all of the information needed to characterize the source. For the simulation of ground motion for a future earthquake, the slip distribution is generated from a frequency-wavenumber model of slip distribution whose parameters are constrained by the slip models of past earthquakes (Somerville and Abrahamson, 1991). The slip direction on the fault (rake angle) can vary spatially over the fault, and can also vary in time at a given point on the fault. The rise time (slip velocity) is based on an empirical relation derived from the same ten events. The rupture velocity is assumed to be 0.85 times the shear wave velocity. Radiation pattern and fault subevents are treated differently in two different period ranges.

Long Period: The fault is discretized finely enough to produce a continuous plane for frequencies below one second. The theoretical radiation pattern is used.

Short Period: The fault is discretized into fault elements. The size of the fault elements is chosen so as to maintain self-similarity in the spectral shape between the subevent on the fault element and the large event based on an omega-squared scaling relation (Joyner and Boore, 1986), as described by Somerville et al. (1991). The condition is that the total number of

subevents added be the four-thirds power of the moment ratio of the large event to the subevent.

The radiation of seismic waves from these fault elements is represented by empirical source functions, which are accelerograms of events having the dimensions of the fault elements that were recorded near the source and have been corrected back to the source. Where multiple empirical source functions are available, the radiation pattern is represented empirically using these source functions, by selecting recordings having the required theoretical radiation pattern value for each fault element.

Path

For 1D models of crustal structure, path effects are treated differently in two different period ranges.

Long Period: Path effects are represented by Green's functions calculated using an efficient frequency-wavenumber integration scheme (Saikia, 1994). In the frequency-wavenumber integration method, the solutions due to a point source are expressed in terms of a double integral transformation over horizontal wavenumber and frequency by taking temporal and spatial Fourier transforms. For a stack of homogeneous plane layers, the kernel of the integrand is expressed by the propagator matrix. The integral of the kernel over the horizontal wavenumber is carried out numerically at a sequence of different frequencies. Time domain solutions are obtained by an inverse Fourier transform. These Green's functions contain the complete response of the layered medium (all body wave and surface wave phases) for frequencies below a given value (typically chosen to be 5 Hz). They also contain the near-field term in addition to the far-field term, and include the static displacement field of the earthquake. The Green's functions include the effects of a layered Q model.

Short Period: Path effects are represented by simplified Green's functions calculated using generalized ray theory (Helmberger, 1983). These Green's functions are accurate up to indefinitely high frequencies (typically 50 Hz), and contain all of the significant rays. They are simplified in the sense that they do not include the radiation pattern and the receiver function; these are excluded because they are represented empirically in the empirical source functions. The simplified Green's functions are used to transfer the empirical source functions from the depth, horizontal range and velocity structure in which they were recorded to the depth, horizontal range and velocity structure in which they are to be used for ground motion simulation. Scattering effects in the path are represented empirically by wave propagation effects contained in the source functions that are not modeled by the simplified Green's functions used in their correction.

Geometrical ray theory breaks down when there are strong velocity gradients. For calculating the propagation of seismic waves in a layered crust, we need to use generalized ray theory which includes refracted arrivals (head waves) as well as reflected arrivals. In the generalized ray method, the kernel of a double integral transformation is obtained by taking a

Laplace transform over time and a spatial Fourier transform over horizontal coordinate. Then, by introducing ray parameter and a relationship between the ray parameter and travel time (Cagniard path), the integral of the kernel which corresponds to an inverse Laplace transform is analytically carried out in order to obtain a time domain solution. The method of generalized rays allows separation of the wavefield into energy that radiates downward and energy that travels upward. To illustrate generalized rays, we describe the decomposition of the wavefield into the following three travel paths:

- (1) direct arrival plus surface layer multiples (shallow Love waves);
- (2) downgoing (diving) energy paths (lower crustal triplications); and
- (3) surface reflected paths which are reflected again below the source (sS).

A smooth velocity model composed of approximately 50 layers is shown in Figure A1-2. This figure also displays two generalized ray sets used in constructing the wavefield: the downgoing ray set and the upgoing ray set (excluding the direct arrival). The upper portion of Figure A1-3 displays the various contributions of these three ray sets to the total potential field. These three contributions are the direct ray, a large set of downgoing rays that are reflected back to the surface, and a large set of upgoing rays that are reflected at the surface and are reflected or refracted back to the surface. These responses were produced by applying the Cagniard-de Hoop technique to the generalized rays (Helmberger, Engen & Grand 1985). These three contributions dominate the wavefield, as can be demonstrated by generating complete synthetic seismograms by the reflectivity method (Saikia, 1994). The upper row shows the decrease in short-period energy with increasing distance as the waves become diffracted. The downgoing rays (or diving rays) contribute significantly to the short period content. The Moho reflection S_mS and the Moho refracted wave S_n (head wave) produce further complexity, especially due to contributions from sS .

Path effects are treated in one of two different methods in 2D crustal models. One method uses generalized rays (Helmberger et al., 1995), and is accurate up to indefinitely high frequencies (typically to 50 Hz). The other method uses finite difference (Helmberger and Vidale, 1988), and contains all body wave and surface wave arrivals for periods longer than a specified cutoff period. This method can also be used for 3-D crustal models.

Site

Site effects are incorporated by calculating Green's functions using the velocity model appropriate for the site. For the short period part of the simulation, the receiver function is included empirically in the empirical source functions; the partitioning of energy among components is treated in a site-specific manner by applying a receiver function correction to the empirical source functions which rotates the recorded partition into that appropriate to the velocity structure at the site. Scattering effects near the site are represented empirically by wave propagation effects contained in the empirical source functions that are not modeled by the simplified Green's functions used in their correction. The site attenuation (κ) contained in the empirical source functions is adjusted to provide the value that is appropriate at the site.

Non-linear effects can be included in an approximate way by using a 1-D equivalent linear approach.

Parameters Requiring Specification

Source: Seismic moment, fault length, fault width, strike, dip, rake, depth of top of fault, hypocenter, rupture velocity, the time function of slip at each point on the fault, and the direction of slip on the fault.

Path: Seismic velocities, density, and Q (material damping factor) of a crustal model that may be plane layered (1D), 2D or 3D. The most sensitive parameters are velocity gradients in the shallow and deep parts of the crust.

Site: Surface seismic velocities, density, and Q (material damping factor). If nonlinear soil response is to be included, we need shear modulus and damping as a function of strain level.

Important Features of the Broadband Ground Motion Simulation Method

As determined from validation against recorded data documented below, the ground motion method is broadband (zero frequency to 50 Hz); is applicable for magnitudes in the range of 5 to 8; and is applicable to distances from 0km to 200km or more. It has no free parameters when used to model the recorded ground motions of an earthquake, and hence no calibration of the model is required. The model has been extensively validated against the recorded strong ground motions of crustal earthquakes using flat layered (1-D) crustal models and more complex (2-D and 3-D) models. At long periods, it contains a theoretically rigorous representation of radiation pattern, rupture directivity and wave propagation effects, and reproduces the recorded ground motion waveforms. At short periods, it uses a theoretically rigorous representation of wave propagation effects which is combined with theoretically-based semi-empirical representations of stochastic processes including source radiation pattern and scattering in the path and site.

The broadband simulation method is based on standard time-domain methods for estimating earthquake source parameters and analyzing seismic wave propagation, and can therefore be readily applied using standard parameterizations of the earthquake source and crustal structure. It has been extensively validated against recorded strong ground motions from both tectonically active regions and tectonically stable regions. It has no free parameters when used to model the recorded ground motions of an earthquake, and hence no calibration of the model is required. The ground motion attenuation function is determined by the crustal structure and the source depth, and thus has predictive power in locations where crustal structure and source depth are available but few strong motion recordings exist. The method can include Green's functions calculated using 2-D or 3-D models of crust structure.

Validation of the Broadband Strong Motion Simulation Method Against Recorded Data

The ground motion model has no free parameters when used to model the recorded ground motions of an earthquake, and hence no calibration of the model is required. The 1-D ground motion model has been validated against the recorded strong ground motions of the following earthquakes: 1978 Tabas (Saikia, 1994); 1979 Imperial Valley (Wald et al., 1988a); 1985 Michoacan, Mexico and Valparaiso, Chile (Somerville et al., 1991); 1987 Whittier Narrows (Wald et al., 1998b; Saikia, 1992); 1988 Saguenay (Somerville et al., 1990; Atkinson and Somerville, 1994); 1988 Nahanni (PG&E, 1988); 1989 Loma Prieta (Somerville et al., 1994a,b); 1994 Northridge (Somerville et al., 1995). The 2-D and 3-D modeling approach, which to date has been applied at periods of 1 sec and longer, has been applied to the ground motions of a Loma Prieta aftershock recorded in the Marina District basin in San Francisco (Graves, 1993); to the ground motions of the 1992 Cape Mendocino earthquake recorded in the Eel River Valley (Graves, 1994a); to the ground motions of the 1994 Northridge earthquake recorded in the northwestern Los Angeles basin (Graves, 1994b); and to the ground motions of the 1995 Kobe earthquake recorded in the Kinki district (Somerville and Graves, 1996).

Uncertainty in Ground Motions Generated using the Broadband Procedure

The uncertainty in ground motions predicted by the model is characterized by the procedure described by Abrahamson et al. (1990). There are two kinds of uncertainty in modeling ground motion, and each contributes about equally to the overall uncertainty. One is variability due to modeling uncertainty associated with the modeling procedure. The other source of uncertainty is that associated with uncertainty in the parameters of future earthquakes. These parameters include the slip distribution, the location of the hypocenter, the slip velocity and the rupture velocity.

The modeling uncertainty is estimated from comparison between recorded and simulated ground motions of earthquakes for which estimates of all of the parameters required by the model are available. The goodness of fit measurement is described by two parameters: the bias and the standard error. In this formulation, the bias measures the difference between recorded and simulated motions averaged over all stations, and provides an indication of whether, on average, the simulation procedure is overpredicting, underpredicting, or evenpredicting the recorded motions. The standard error measures the average difference between the simulated and recorded motions for a single observation, and provides an indication of the uncertainty involved in predicting a single value. The average of all these errors, which include both overprediction and underprediction, is the bias. The standard error in the prediction of a single observation (response spectral velocity at 5% damping) is about a factor of 1.4 (natural logarithm of standard error = 0.35) in the period range of 0.05 to 10 seconds. .

References

Abrahamson, N.A., P.G. Somerville, and C.A. Cornell (1990). Uncertainty in numerical strong motion predictions. *Proc. Fourth U.S. Nat. Conf. Earthq. Eng., Palm Springs, CA*, 1, 407-416.

Atkinson, G.M. and P.G. Somerville (1994). Calibration of time history simulation methods, *Bull. Seism. Soc. Am.* 84, 400-414.

Graves, R.W. and P.G. Somerville (1995). Characterization of long period (1-10 sec) ground motions for base isolated structures located in sedimentary basins. Seismic, Shock and Vibration Isolation, PVP-Vol. 319, Proceedings of the 1995 Joint ASME/JSME Pressure Vessels and Piping Conference, Honolulu, Hawaii, July 23-27, 1995.

Graves, R.W. (1993). Modeling three-dimensional site response effects in the Marina District basin, San Francisco, California.

Graves, R.W. (1994a). Simulating the 3D basin response in the Portland and Puget Sound regions from large subduction zone earthquakes, Annual Technical Report to USGS, Award 1434-93-G-2327.

Graves, R.W. (1994b). Preliminary analysis of long-period basin response in the Los Angeles region from the 1994 Northridge earthquake, *Geophys. Res. Lett.*, 22, 101-104.

Helmberger, D.V., G. Engen and S. Grand (1985). Notes on wave propagation in laterally varying structure, *J. Geophys. Res.* 58, 82-91.

Helmberger, D.V. (1983). Theory and application of synthetic seismograms. in *Earthquakes: Observation, Theory and Interpretation*, Proc. Int. Sch. Phys. "Enrico Fermi" Course LXXXV, pp. 174-221, eds. Kanamori, H. and E. Boschi, North-Holland, Amsterdam.

Helmberger, D.V., R. Stead, P. Ho-Liu, and D. Dreger (1992). Broadband modeling of regional seismograms: Imperial Valley to Pasadena, *Geophys. J. Int.* 110, 42-54.

Helmberger, D.V. and J.E. Vidale (1988). Modeling strong motions with two-dimensional numerical codes, *Bull. Seism. Soc. Am.* 78, 109-121.

Helmberger, D.V., L.-S. Zhao, and E. Garnero (1995). Construction of synthetic seismograms for 2D structures: core phases, in *Earthquakes: Observation, Theory and Interpretation*, n. LXXV, Corso, Italiana di Fisica - Bologna, Italy, in press.

Joyner, W.B. and D.M. Boore (1986). On simulating large earthquakes by Green's function addition of smaller earthquakes, in *Earthquake Source Mechanics*, D. Das, J. Boatwright, and C.H. Scholz

Pacific Gas & Electric Company (1988). Final Report of the Diablo Canyon Long Term Seismic Program for the Diablo Canyon Power Plant, Report to the U.S.N.R.C.

Saikia, C.K. (1993). Estimated ground motions in Los Angeles due to a M=7 earthquake on the Elysian thrust fault, *Bull. Seism. Soc. Am.* 83, 780-810.

Saikia, C.K. (1994). Modeling of strong ground motions from the 16 September 1978 Tabas, Iran, Earthquake, *Bull. Seism. Soc. Am.* 84, 31-46.

Saikia, C.K. (1994). Modified frequency-wavenumber algorithm for regional seismograms using Filon's quadrature: modeling of Lg waves in eastern North America. *Geophys. J. Int.* 118, 142-158.

Somerville, P.G. (1992). Engineering applications of strong motion simulation, *Tectonophysics*, 218, 195-219.

Somerville, P.G., J.P. McLaren, L.V. LeFevre, R.W. Burger, and D.V. Helmberger (1987). Comparison of source scaling relations of eastern and western North American earthquakes, *Bull. Seism. Soc. Am.* 77, 322-346.

Somerville, P.G., J.P. McLaren, C.K. Saikia, and D.V. Helmberger (1990). The 25 November, 1988 Saguenay, Quebec earthquake: source parameters and the attenuation of strong ground motion, *Bull. Seism. Soc. Am.* 80, 1118-1143.

Somerville, P.G., M.K. Sen and B.P. Cohee (1991). Simulation of strong ground motions recorded during the 1985 Michoacan, Mexico and Valaparaíso, Chile earthquakes, *Bull. Seism. Soc. Am.* 81, 1-27.

Somerville, P.G. and N.A. Abrahamson (1991). Characterizing earthquake slip models for the prediction of strong ground motions, *EOS* 72, 341. (abstract).

Somerville, P.G., K. Irikura, S. Sawada, Y. Iwasaki, M. Tai and M. Fushimi (1993). Characterizing earthquake slip models for the prediction of strong ground motion. Proceedings of the 22nd JSCE Earthquake Engineering Symposium - 1993, Japan Society of Civil Engineers, p. 291-294.

Somerville, P.G., D.J. Wald, and N.F. Smith (1994a). Prediction of near fault ground motions of the 1989 Loma Prieta earthquake using a heterogeneous slip model, unpublished manuscript.

Somerville, P.G., N.F. Smith and R.W. Graves (1994b). The effect of critical Moho reflections on the attenuation of strong motion from the 1989 Loma Prieta, in *"The Loma Prieta, California, Earthquake of October 17, 1989 - Strong Ground Motion,"* U.S.G.S. Professional Paper 1551-A, A67-A75.

Somerville, P.G., R.W. Graves, and C.K. Saikia (1995). Characterization of Ground Motions during the Northridge Earthquake of January 17, 1994. Program to Reduce the Earthquake Hazards of Steel Moment Frame Buildings, SAC Report 95-03.

Somerville, P., C. Saikia, D. Wald, and R. Graves (1996). Implications of the Northridge earthquake for strong ground motions from thrust faults, *Bull. Seism. Soc. Am.* 86, S115-S125.

Somerville, P.G. and R.W. Graves (1996). Strong ground motions of the Kobe, Japan earthquake of Jan. 17, 1995, and development of a model of forward rupture directivity applicable in California. Proceedings of the Western Regional Technical Seminar on Earthquake Engineering for Dams, Association of State Dam Safety Officials, Sacramento, California, April 11-12, 1996.

Wald, D.J., L.J. Burdick and P.G. Somerville (1988a). Simulation of acceleration time histories close to large earthquakes. *Earthquake Engineering and Soil Dynamics II - Recent Advances in Ground Motion Evaluation*, Geotechnical Special Publication 20, J. Lawrence Von Thun, ed., 430-444.

Wald, D.J., P.G. Somerville and L.J. Burdick (1988b). Simulation of recorded accelerations of the 1987 Whittier Narrows earthquake, *Earthquake Spectra* 4, 139-156.

Wald, D.J. and T.H. Heaton (1994). Spatial and temporal distribution of slip for the 1992 Landers, California earthquake. *Bull. Seism. Soc. Am* 84, 668-691.

Matched Filters Used for Broadband Simulation

Corner Periods = 3.0 sec

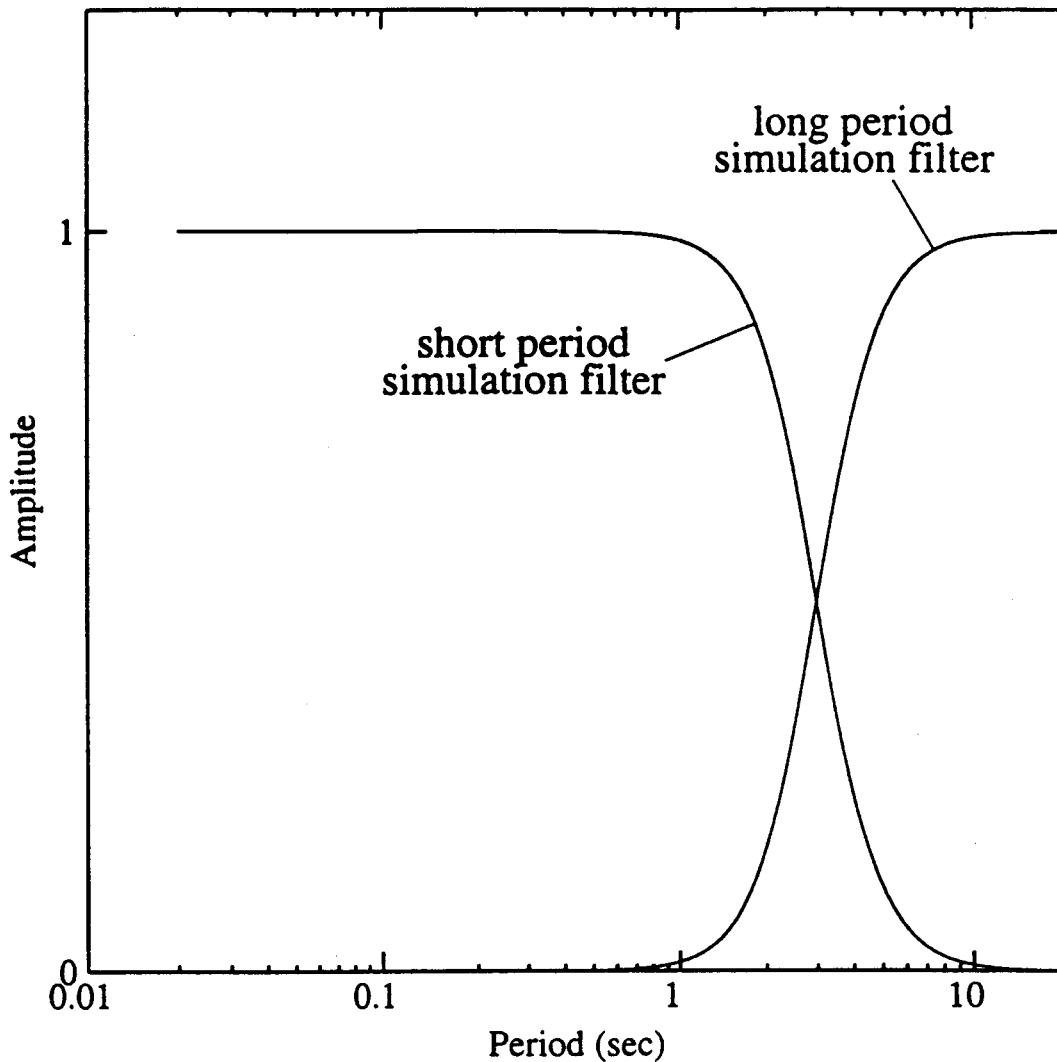


Figure A1-1. Schematic diagram showing the matched filters used to combine the short period and long period simulations. The sum of the matched filters is unity at all periods.

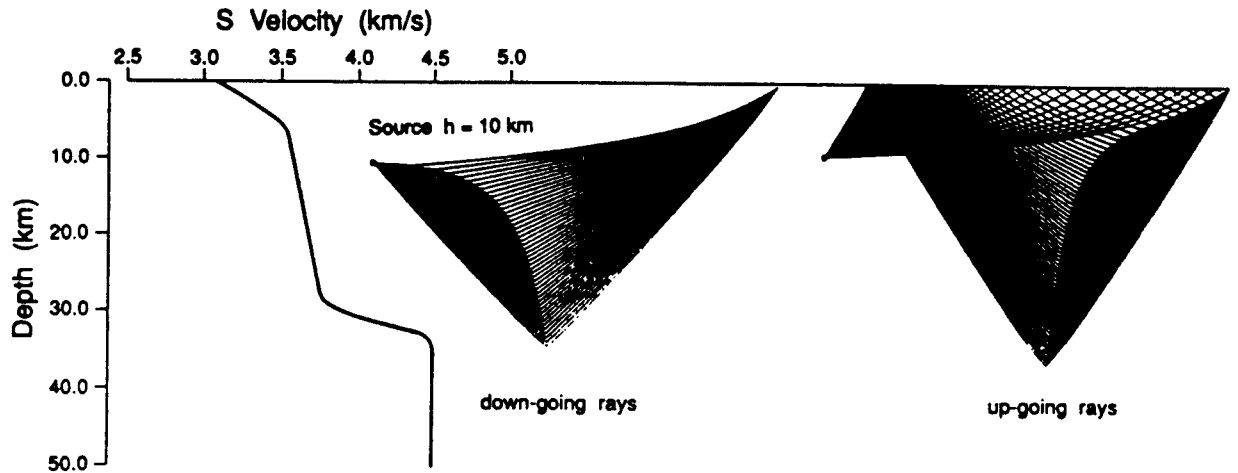


Figure A1-2. A smooth velocity-depth function and generalized ray paths used to construct the synthetic seismograms shown in Figure A1-3. Source: Helmberger et al. (1992).

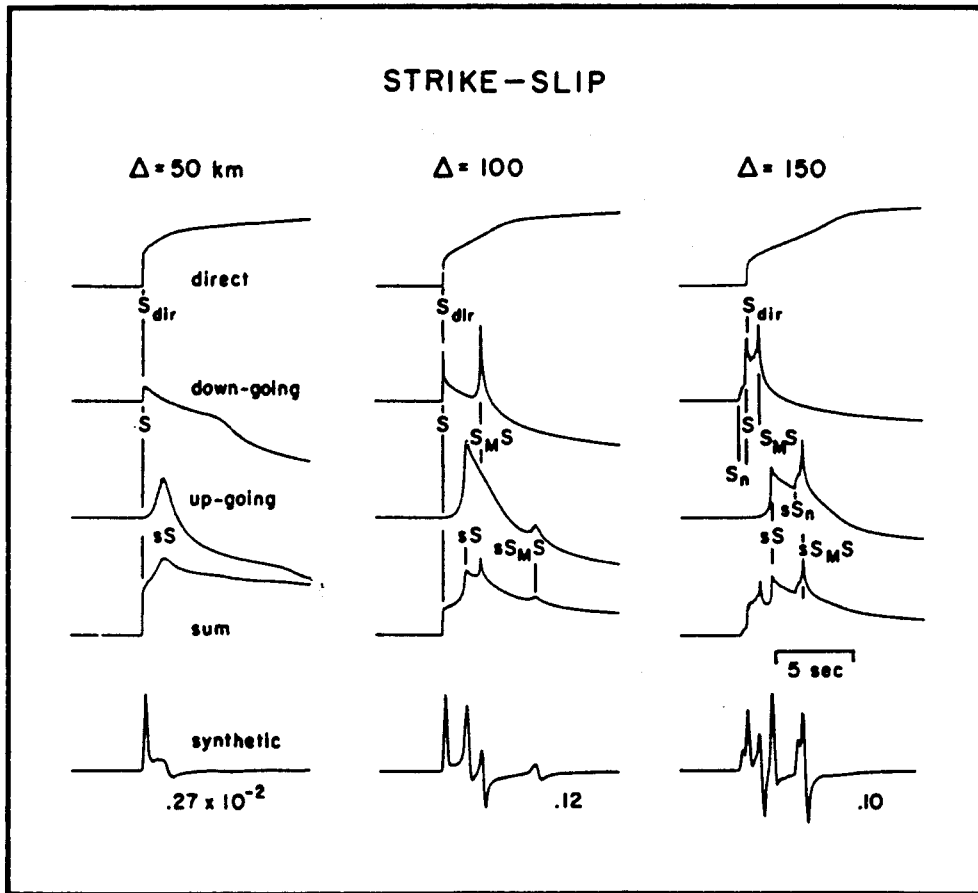


Figure A1-3. Wavefield decomposition showing the response of the direct arrival at the top followed by the contribution from downgoing paths (S) and upgoing paths (sS). The bottom row shows synthetic seismograms computed using a (0.2, 0.2, 0.2) second trapezoidal source. Source: Helmberger et al. (1992).

ACKNOWLEDGEMENTS

The work described in this report was funded by the Pacific Earthquake Engineering Research (PEER) Center under the Pacific Gas & Electric Company Contract No. 09566. This financial support is gratefully acknowledged.

The financial support of the PEARL sponsor organizations including the Pacific Gas & Electric Company (PG&E), the California Energy Commission (CEC), and the California Department of Transportation (Caltrans) is acknowledged.